Bull. Mater. Sci., Vol. 36, No. 5, October 2013, pp. 907–911. © Indian Academy of Sciences.

Sintering behaviour and mechanical properties of Cr_3C_2–NiCr cermets

A ÖZER* **and Y K TÜR**
Department of Material Science and Engineering, Gebze Institute of Technology, Gebze, Kocaeli, Turkey

MS received 20 January 2012; revised 11 July 2012

Abstract. **Cr_3C_2–NiCr cermets are used as metal cutting tools due to their relatively high hardness and low sintering temperatures. In this study, a powder mixture consisting of 75 wt% Cr_3C_2–25 wt% NiCr was sintered at four different temperatures and characterized for its microstructure and mechanical properties. The highest relative density obtained was 97% when sintered at 1350 °C. As the relative density increased, elastic modulus, transverse rupture strength, fracture toughness and hardness of the samples reached to a maximum of 314 GPa, 810 MPa, 10·4 MPa·$m^{1/2}$ and 11·3 GPa, respectively. However, sintering at 1400 °C caused further grain growth and pore coalescence which resulted in decreasing density and degradation of all mechanical properties. Fracture surface investigation showed that the main failure mechanism was the intergranular fracture of ceramic phase accompanied by the ductile fracture of the metal phase which deformed plastically during crack propagation and enhanced the fracture toughness.**

Keywords. **Cermet; Cr_3C_2–NiCr; sintering; mechanical properties.**

1. Introduction

Chromium carbide–nichrome (Cr_3C_2–NiCr) cermets are widely employed in wear resistant applications involving sliding, abrasion and erosion over a wide range of temperatures (Murthy *et al* 2007). The interest in these materials is due to their high corrosion resistance as compared to WC–Co/Ni or TiC–Mo (Pirso *et al* 2006); therefore, they are known as stainless steel of cutting tools (Kayuk *et al* 2007). Duran and Eroglu (1998) investigated the effect of Cr_3C_2 content on green density, sintering behaviour, hardness and microstructure. They also studied the effect of different binders such as NiCr, NiFe on the densification behaviour and microstructures of Cr_3C_2-based cermets (Eroglu and Duran 1997). Hussainova *et al* (2007) investigated the effect of Ni content on the wear behaviour of Cr_3C_2-based cermets and found that the wear rate decreases with an increase in hardness due to decreasing Ni content. Chauhan *et al* (2010) evaluated the high impact angle erosion wear characteristics of Cr_3C_2–NiCr and WC–Co cermets coatings, comparatively. 75Cr_3C_2–25NiCr coatings showed higher wear resistance than WC–Co coatings at 90° due to good binder wettability and high ductility of the binder phase which prevent further material removal (Chauhan *et al* 2010). Huang *et al* investigated the mechanical properties of VC, Cr_3C_2 and NbC doped WC–Co cermets and found that pure WC–Co cermet had a lower hardness than that of doped cermet. Pure WC–Co cermets had a higher fracture toughness than that of doped ones (Huang *et al* 2007, 2008).

At the light of above discussions, determining the fracture toughness, understanding the fracture behaviour of Cr_3C_2–NiCr cermets and establishing a microstructure–toughness relation still need further study. In a step towards this, 75 wt% Cr_3C_2–25 wt% NiCr specimens were sintered at different temperatures in order to study their densification behaviour and mechanical properties. The effect of microstructure and relative density on the elastic modulus, transverse rupture strength, fracture toughness and hardness of Cr_3C_2–NiCr cermets is investigated.

2. Materials and methods

Cr_3C_2, Ni, and Cr were obtained in powder form from Atlantic Equipments Co. Inc. USA. Mean diameters of the particles (d_{50}) were measured to be 1·7, 8·5 and 4·2 μm for Cr_3C_2, Ni and Cr, respectively. 75 wt% Cr_3C_2–20 wt% Ni–5 wt% Cr powder mixture with a Ni:Cr ratio of 4:1 by weight was prepared by wet ball milling for 6 h. Methyl ethyl ketone–ethanol solution (Mek/EtOH) was used as a wet medium.

The ceramic-metal powder mixture was pressed uniaxially under a pressure of 60 MPa and then cold-isostatically pressed under a pressure of 100 MPa. The relative densities of the green compacts were around 62% prior to sintering.

The compacted specimens were heated up to sintering temperatures ranging from 1260 to 1400 °C with a heating rate of 5 °C/min. They were held at the sintering temperatures for 30 min and then cooled to room temperature

*Author for correspondence (aozer@gyte.edu.tr)

in the furnace with a cooling rate of 10 °C/min, approximately. Sintering process was carried out under flowing argon.

The bulk density measurements of the sintered samples were done by the Archimedes immersion method. The samples, in prismatic shape with dimensions of 25 × 3·5 × 4 mm, were polished down to 3 μm to eliminate the effect of surface flaws on mechanical properties. Elastic modulus was measured using impulse excitation technique (GrindoSonic® Mk5) in accordance with ASTM E-1876-94 standards. Hardness was measured by an Instron® Wolpert Testor 2100 equipped with a diamond pyramid Vickers indenter. Loading time and load was selected as 10 s and 10 kg, respectively. Transverse rupture strength (TRS) and fracture toughness tests were performed by Instron® 5569 Universal Test Device at a crosshead speed of 0·05 mm/min and a loading span of 20 mm. Pre-notched fracture tests were carried out to evaluate fracture toughness of the fabricated cermet specimens. The pre-notch was cut on 3·5 × 25 mm face such that $0{\cdot}33\,h < a < 0{\cdot}5\,h$, where a is the notch depth and h the specimen height. The notch depths were measured after fracture. Fracture toughness, K_{IC}, was estimated by (1) (Mencik 1992).

$$K_{IC} = \frac{3Fl\sqrt{a}}{2bh^2}\left(1.93 - 3.07q + 14.53q^2 - 25.11q^3 + 25.80q^4\right), \quad (1)$$

where F is the fracture load, b the specimen width, l the load span and $q = a/h$. The microstructural and fracture surface characterization of the cermets were carried out using a scanning electron microscope (SEM) (Philips XL30-FEG) in back scattered electron imaging (BSE) and secondary electron imaging (SEI) mode. Energy dispersive spectrometry (EDS) analysis was also carried out to determine the relative amount of elements in microstructure.

3. Results and discussion

Sintering temperatures were selected according to the reported differential thermal analysis (DTA) (Duran and Eroglu 1998), indicating that 1260 and 1300 °C were the temperatures below and above the liquid metal formation temperature, respectively. Therefore, 1350 °C was chosen for full densification and 1400 °C for identifying further consolidation of 75 wt% Cr_3C_2–25 wt% NiCr(4:1) cermets, for grain growth and pore coalescence characteristics.

An XRD pattern obtained from cermet samples sintered at four sintering temperatures can be seen in figure 1. The main peak of Ni(Cr) which diffracts from (111) plane shifted to left by increasing temperature due to increasing dissolution of Cr and Cr–C phases in Ni lattice which further increase the lattice parameter of Ni. Cr_3C_2 is the main ceramic phase but the formation of another orthorhombic phase, Cr_7C_3, is inevitable by increasing temperature from 1300 to 1350 °C and 1400 °C. This may be attributed to transportation of Cr and C atoms at different speeds in the liquid phase that results in stoichiometric changes.

Figure 2 shows SEM images of the samples sintered at four different temperatures. At 1260 °C (figure 2a), due to solid state sintering, only the neck formation between particle contact regions was observed. At this stage, surface diffusion and evaporation–condensation were the two active material transport mechanisms between the particles which yielded no significant densification. At 1300 °C (figure 2b), a slight increase in relative density from 67% to 76% was observed due to enhanced diffusional activities in grain boundary regions which resulted in neck growth. Figure 2(c) shows that the growth of the faceted grains and the densification were remarkably promoted by the liquid phase formation at 1350 °C. The densities as high as 97% of the theoretical density have been achieved by liquid phase sintering through the solution–reprecipitation and grain

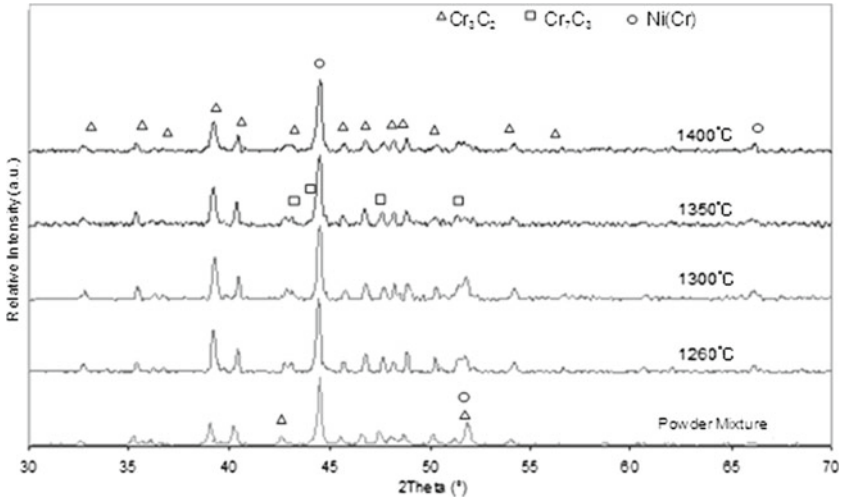

Figure 1. XRD pattern of powder mixture and cermet samples sintered at four temperatures.

boundary diffusion mechanisms. Liquid phase dissolves small particles and reduces particle–particle contact pressures by transferring the material to low pressured regions. It also causes rounding of grain edges as observed in figure 2(c).

Upon increase in the sintering temperature to 1400 °C, further grain growth is evident from the microstructure as shown in figure 2(d). Particle size measurements were conducted on SEM images (figures 2c and d). At 1350 °C sintering temperature, the average grain dimensions were 4·0 × 6·4 μm with an aspect ratio of 1·6. In comparison, at 1400 °C sintering temperature, the average grain dimensions increased 5·2 × 9·5 μm with an aspect ratio of 1·9. Grain growth can be attributed to higher diffusion rate and grain faceting of orthorhombic Cr_3C_2 crystals allowed grains to grow more rapidly.

SEM-EDS analysis of the cermets sintered at 1350 and 1400 °C was conducted and distinct regions were shown by letters A, B and C in figures 2(c) and (d). Dark gray (A) and light gray (B) regions indicate Cr rich phase which correspond to Cr_3C_2 grains. EDS analysis showed that dark gray regions did not contain Ni while light gray grains are a mixture of Ni (20 wt% Ni) and Cr_3C_2 (80 wt% Cr) phases. White regions (C) represent Ni based binder phase (75 wt% Ni–25 wt% Cr).

It is well known that density is one of the major parameters that affect mechanical properties of ceramic materials. Figure 3 shows that up to 1350 °C, the relative density, elastic modulus, transverse rupture strength (TRS), fracture toughness and hardness increase with increase of the sintering temperature. Their peak values are 97%, 314 GPa, 810 MPa, 10·4 MPa·m$^{1/2}$ and 11·3 GPa, respectively. Sintering at 1400 °C decreased the relative density to 94% because of the increase in pore sizes and total porosity while the number of pores decreased. Further grain growth by pore coarsening causes a decrease in relative density. This phenomena is known as the de-densification. Figure 3 shows a decrease in all mechanical properties at 1400 °C.

Figure 4 shows SEM images of the fracture surfaces of the samples sintered at four different temperatures. At 1260 °C (figure 4a), discrete ceramic grains connected by a metallic phase were observed in the microstructure. A neck growth by a solid state sintering is also present. The fracture morphology is a mixture of intergranular fracture of the ceramic phase at the grain boundaries and ductile fracture of the metallic phase by necking. Although intergranular fracture played a major role, the fracture toughness remained as high as 4·6 MPa·m$^{1/2}$ due to the ductile fracture of the binding metal phase. As the sintering temperature increased, an increase in relative density and a decrease in porosity were determined although it was not clearly evident from the microstructure in figure 4(b). At this stage, the relative density reached to 76%. The contribution of the metal phase to the mechanical properties did not show a significant change but a slight increase in the fracture toughness was determined increasing its value from 4·6 to 6 MPa·m$^{1/2}$.

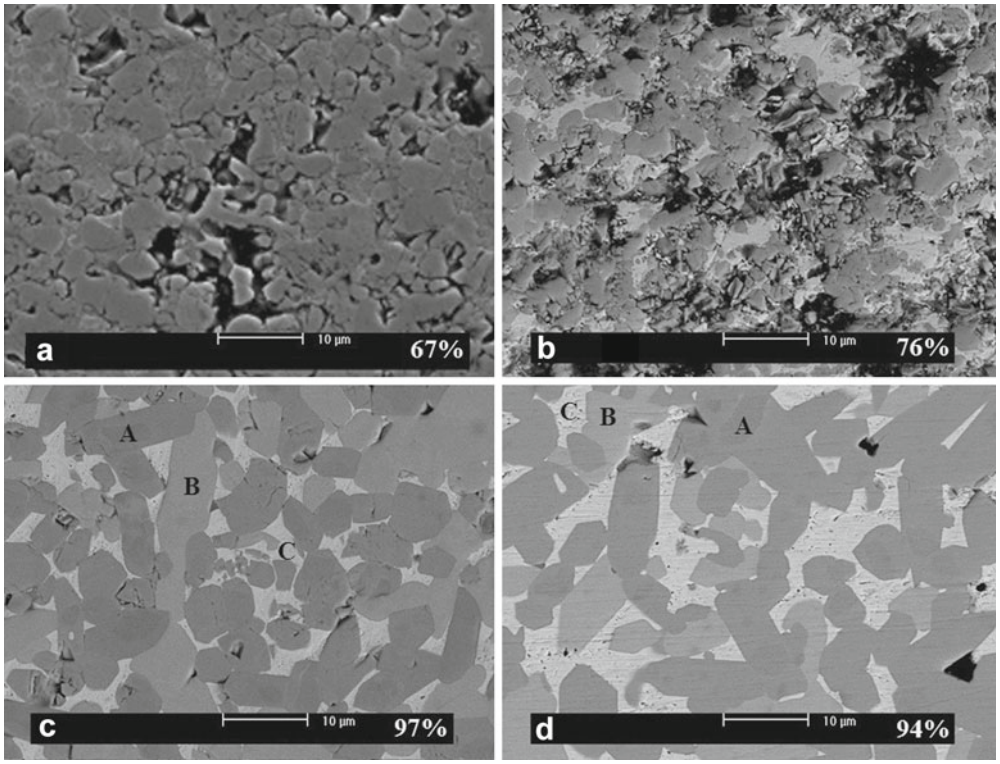

Figure 2. SEM–BSE micrographs of samples sintered at (**a**) 1260, (**b**) 1300, (**c**) 1350 and (**d**) 1400 °C with their respective relative densities. A: Cr_3C_2; B: Cr_3C_2+Ni; C: Ni(Cr).

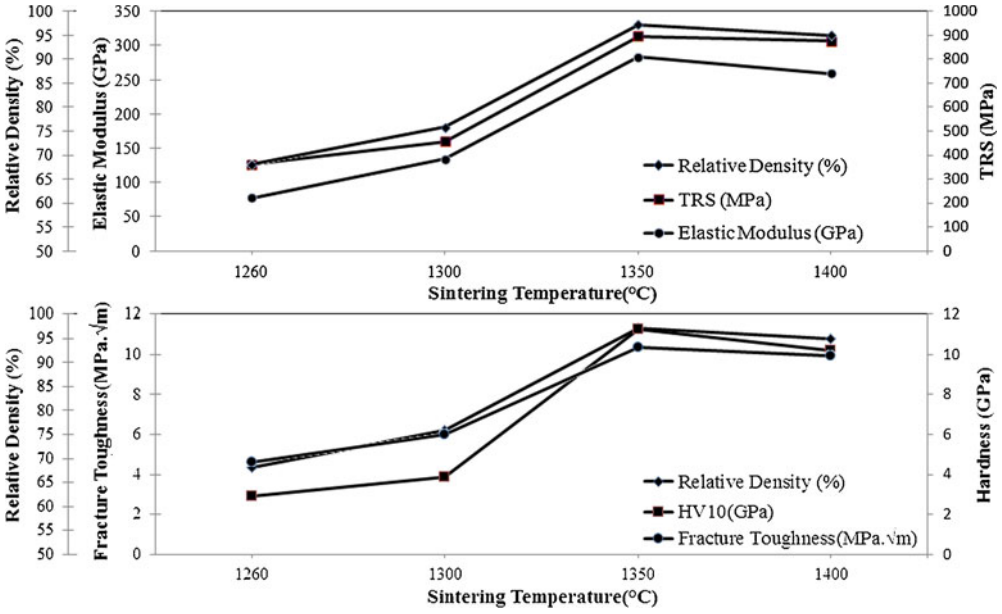

Figure 3. Relative densities and mechanical properties of samples as a function of sintering temperature.

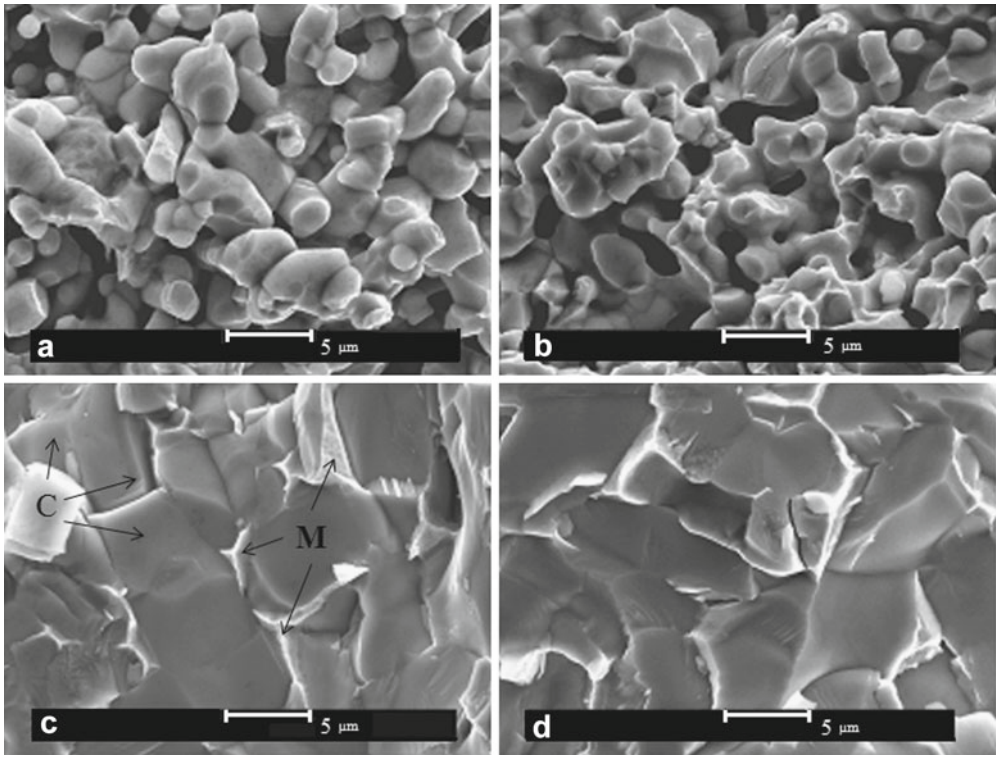

Figure 4. SEM–SEI micrographs of fracture surfaces sintered at (**a**) 1260, (**b**) 1300, (**c**) 1350 and (**d**) 1400 °C.

In figure 4(c), it is seen that maximum densification of the samples was attained at 1350 °C and at this temperature, continuity of the metal phase was achieved, metal–ceramic interface binding was completed, and minimum porosity level was reached. The fracture toughness values reached to a maximum of 10·4 MPa·$m^{1/2}$. This toughness is much higher than those of well known engineering structural ceramics such as alumina, SiC, mullite composites (2–5 MPa·$m^{1/2}$) (Tekeli 2005; Öztürk and Tür 2007); but still less than the SEVNB fracture toughness of WC–Co

cermets (15–20 MPa·$m^{1/2}$) (Torres *et al* 2001). As seen from figure 4(c), metal phase deforms plastically during crack propagation (shown by arrow M). Transgranular and intergranular fracture of ceramic grains (shown by arrow C) indicates that ceramic phase has no significant contribution to the toughness of the specimens. Figure 4(d) shows micrograph of the fracture surface of the specimen sintered at 1400 °C. The fracture mechanisms remain identical, i.e. ductile failure of the metal phase and brittle fracture of the ceramic phase. However, coarsening of the grains at a higher sintering temperature of 1400 °C provided longer uninterrupted crack paths that decreases the fracture toughness to 9·9 MPa·$m^{1/2}$.

For brittle materials, Rice (1996) has stated that the fracture toughness decreases with decreasing relative density. According to Rice, the decrease in toughness may be similar to that for strength and elastic modulus. In our study, it was observed that a 3% decrease in the theoretical density resulted in a 2% decrease in the elastic modulus. However, the accompanying decrease in the fracture toughness was 5%. Besides, the decrease in strength of the specimens was even more pronounced, 8%. Coarsening of the grains at 1400 °C sintering temperature provided longer uninterrupted crack paths, degrading the fracture toughness. A decrease in fracture toughness coupled with an increase in grain size, i.e. effective crack length, resulted in an 8% decrease in the flexure strength of the specimens.

The decrease in hardness was 9% which is similar to the decrease in strength. Besides the decrease in relative density, this decrease in the hardness values is attributed to the larger metal phase regions in the specimens sintered at 1400 °C, as seen in figure 2(c) and (d). These larger metal phase regions deformed more easily because they were less restricted by the ceramic phase; therefore, a much lower hardness was observed.

The maximum relative density obtained in this study was 97% of the theoretical density. Our results indicate that by increasing the relative density of Cr_3C_2–NiCr cermets and by suppressing grain growth of the ceramic phase, an increase in mechanical properties can be achieved, especially in strength and hardness.

As a future study, the effect of additives on densification behaviour of Cr_3C_2–NiCr cermets and wear properties of Cr_3C_2–NiCr cermets are being investigated.

4. Conclusions

The Cr_3C_2–NiCr cermet specimens with a nominal composition of 75 wt% Cr_3C_2–25 wt% NiCr were successfully densified. The sintering temperature of 1350 °C was found to be appropriate temperature for maximum densification by a liquid phase sintering in the present investigation. The specimens sintered at 1350 °C had a relatively high density of 97% and exhibited the best mechanical properties with the values in elastic modulus (314 GPa), transverse rupture strength (810 MPa), fracture toughness (10·4 MPa·$m^{1/2}$) and hardness (11·3 GPa). Fracture surface investigation showed that the main failure mechanism was the transgranular and intergranular fracture of ceramic grains while ductile fracture of the metal phase which deformed plastically during crack propagation can also be observed that enhanced the fracture toughness. Sintering at 1400 °C resulted in grain growth and pore coarsening, which decreased the relative density and consequently deteriorated the mechanical properties. As a result, the elastic modulus decreased slightly. However, the decrease in the fracture toughness, transverse rupture strength and hardness were more pronounced and attributed to the increase in the size of the ceramic grains and larger metal phase regions.

Acknowledgement

The authors would like to thank Mr Ahmet Nazim and Mr Adem Şen for their kind help in SEM imaging and XRD analysis, respectively. The support of GIT Scientific Research Council # 2009-A-22 project is greatly appreciated.

References

Chauhan A K, Goel D B and Prakash S 2010 *Bull. Mater. Sci*. **33** 483

Duran C and Eroglu S 1998 *J. Mater. Process. Technol*. **74** 69

Eroglu S and Duran C 1997 *Scr. Mater*. **37** 991

Huang S G, Li L, Van der Biest O and Vleugels J 2008 *J. Alloys Compds*. **464** 205–211

Hussainova I, Pirso J, Antonov M, Juhani K and Letunovitš S 2007 *Wear* **263** 905

Kayuk V G, Koval'chenko M S, Martsenyuk I S and Grigor'ev O N 2007 *Powder Metall. Metal Ceram*. **46** 228

Li H L, Vanmeensel K, Van der Biest O and Vleugels J 2007 *Int. J. Refract. Metals Hard Mater*. **25** 417

Mencik J 1992 *Strength and fracture of glass and ceramics*, in *Glass science and technology* (Amsterdam: Elsevier)

Murthy J K N, Bysakh S, Gopinath K and Venkataraman B 2007 *Surf. Coat. Technol*. **202** 1

Öztürk C and Tür Y K 2007 *J. Eur. Ceram. Soc*. **27** 1463

Pirso J, Viljus M and Letunovits S 2006 *Wear* **260** 815

Rice R W 1996 *J. Mater. Sci*. **31** 1969

Tekeli S 2005 *J. Alloys Compds* **391** 217

Torres Y, Casellas D, Anglada M and Llanes L 2001 *Int. J. Refract. Metals Hard Mater*. **19** 27